Influence of the Sea Ice Thickness Distribution on Polar Climate in CCSM3

MARIKA M. HOLLAND

National Center for Atmospheric Research, Boulder, Colorado*

CECILIA M. BITZ

Atmospheric Sciences, University of Washington, Seattle, Washington

ELIZABETH C. HUNKE AND WILLIAM H. LIPSCOMB

T-3 Fluid Dynamics Group MS-B216, Los Alamos National Laboratory, Los Alamos, New Mexico

JULIE L. SCHRAMM

National Center for Atmospheric Research, Boulder, Colorado*

(Manuscript received 23 January 2005, in final form 18 August 2005)

ABSTRACT

The sea ice simulation of the Community Climate System Model version 3 (CCSM3) T42-gx1 and T85-gx1 control simulations is presented and the influence of the parameterized sea ice thickness distribution (ITD) on polar climate conditions is examined. This includes an analysis of the change in mean climate conditions and simulated sea ice feedbacks when an ITD is included. It is found that including a representation of the subgrid-scale ITD results in larger ice growth rates and thicker sea ice. These larger growth rates represent a higher heat loss from the ocean ice column to the atmosphere, resulting in warmer surface conditions. Ocean circulation, most notably in the Southern Hemisphere, is also modified by the ITD because of the influence of enhanced high-latitude ice formation on the ocean buoyancy flux and resulting deep water formation. Changes in atmospheric circulation also result, again most notably in the Southern Hemisphere.

There are indications that the ITD also modifies simulated sea ice–related feedbacks. In regions of similar ice thickness, the surface albedo changes at $2XCO_2$ conditions are larger when an ITD is included, suggesting an enhanced surface albedo feedback. The presence of an ITD also modifies the ice thickness–ice strength relationship and the ice thickness–ice growth rate relationship, both of which represent negative feedbacks on ice thickness. The net influence of the ITD on polar climate sensitivity and variability results from the interaction of these and other complex feedback processes.

1. Introduction

The Arctic region is important in that there are feedback mechanisms associated with changes in snow and sea ice which amplify climate change and variability. In increasing atmospheric CO_2 scenarios, an amplified warming at high latitudes is seen largely due to the changes in sea ice (e.g., Houghton et al. 2001). However, at transient $2XCO_2$ conditions, the magnitude of this amplification varies considerably among different climate models. Holland and Bitz (2003) showed that some of this variation was related to different sea ice control climate conditions. Additionally, the response of clouds and ocean heat transport to changing CO_2 levels contributes to different high latitude warming simulations.

As has been recognized for some time (Robock 1983), parameterizations of sea ice physical processes also influence simulated polar amplification. The role that particular parameterizations play in the simulation of climate feedbacks has been discussed in a number of

* The National Center for Atmospheric Research is sponsored by the National Science Foundation.

Corresponding author address: Dr. Marika Holland, NCAR, P.O. Box 3000, Boulder, CO 80307.
E-mail: mholland@ucar.edu

studies. For example, research using ice-only model simulations suggests that ice dynamics reduces the sensitivity of the ice cover to forcing perturbations (e.g., Hibler 1984; Holland et al. 1993). This happens because of the ice thickness–ice strength relationship in which thicker ice cover has more resistance to convergence and less dynamical thickening. Additionally, single-column modeling studies, suggest that including a subgrid-scale ice thickness distribution reduces simulated ice thickness variability because of the stabilizing influence of resolving the thin ice cover (Holland and Curry 1999). These studies and others highlight the fact that changes in sea ice model physics not only influence the simulated mean state but also modify the ice-cover response to external perturbations.

Sea ice components of global climate models have improved significantly in the last several years. For example, the Community Climate System Model version 3 (CCSM3) has incorporated a parameterization of the subgrid-scale sea ice thickness distribution (ITD). This parameterization represents the high spatial variability that is present in the observed ice cover, allowing for a number of different ice categories within a single model grid cell. Previous studies using single column models (Maykut 1982; Bjork 1992; Schramm et al. 1997; Holland et al. 1997) and models of intermediate complexity (Bitz et al. 2001; Holland et al. 2001) have shown that the ITD is important for simulating Arctic conditions. In particular, resolving thin ice cover within the pack ice influences the sea ice mass budget and ice–ocean–atmosphere exchange. This results in more ice growth and a thicker ice cover when an ITD is included.

The influence of the ITD on ice growth rates and interfacial fluxes also has the potential to modify simulated polar feedbacks. This can result in changes to the climate sensitivity and variability of the system. For example, Bitz et al. (2001) showed that simulated variability in the thermohaline circulation was modified with the inclusion of an ITD.

These previous studies have been instrumental in our understanding of the influence of the ITD on the climate system. However, to date, there has been no study showing the influence of the ITD on simulations of a fully coupled general circulation model. Additionally, there has been little focus on the influence of the ITD on simulating climate feedbacks and polar amplification. Here we address these issues using the CCSM3. We discuss the sea ice simulated in the CCSM3 at two resolutions, T42-gx1 and T85-gx1, with some comparison to observations (section 3). Next, we examine the ITD influence on the mean climate conditions in both fully coupled and atmosphere–ice slab ocean model runs (section 4). Finally, we examine the influence of the ITD on simulating sea ice feedbacks (section 5), including the surface albedo feedback, the ice thickness–ice growth rate feedback, and ice dynamic feedbacks. We present a discussion and conclusions in section 6.

2. Model description and experimental design

a. Model description

The CCSM3 is a fully coupled, state-of-the-art general circulation model. Collins et al. (2006a) give an overall description of the model and its mean climate. Other papers in this issue describe the model physics and climate simulations in detail. Here we discuss the main features of the Community Sea Ice Model (CSIM), the sea ice component of CCSM3. A full description is given by Briegleb et al. (2004), which can be downloaded from http://www.ccsm.ucar.edu/models/ccsm3.0/csim.

CSIM is a dynamic–thermodynamic model that includes a subgrid-scale ITD. The governing equation for the ITD (Thorndike et al. 1975) is

$$\frac{\partial g}{\partial t} = -\frac{\partial}{\partial h}(fg) + L(g) - \nabla \cdot (\mathbf{v}g) + \Psi(h, g, \mathbf{v}), \quad (1)$$

where h is the ice thickness, f is the rate of change of ice thickness due to thermodynamic processes, $\mathbf{v}$ is the 2D ice velocity, $\nabla \cdot (\mathbf{v}g)$ is the horizontal divergence, Ψ is the redistribution function, and g is the ice thickness distribution, with $g(h)dh$ defined as the fractional area covered by ice of thickness h to $h + dh$. The second term on the rhs represents lateral melting and ice formation, and the last term represents mechanical redistribution by rafting and ridging.

Equation (1) is discretized in thickness space by dividing the ITD into N categories, each with a prescribed thickness range, plus an open water category. The equation is solved in stages. First, the thermodynamic scheme computes the growth rate f, which gives a new set of category thicknesses. Ice is transported in thickness space to neighboring categories (the first term on the rhs) and then is grown or melted laterally (the second term). Next, the dynamics scheme computes the velocity, $\mathbf{v}$. Ice is transported horizontally (the third term) and finally is mechanically redistributed among categories (the fourth term).

Vertical growth and melting are computed using the energy-conserving thermodynamic scheme of Bitz and Lipscomb (1999), which is based on the work of Maykut and Untersteiner (1971). The model has multiple ice layers (typically four) and a single snow layer. A vertical salinity profile is prescribed to account for brine pockets, which modify the conductivity and specific

heat of the ice. Each ice layer has an enthalpy, defined as the energy needed to completely melt a unit mass of brine-filled ice. The enthalpy is a function of the prognostic temperature and prescribed salinity. Temperature changes are given by a vertical heat diffusion equation, which is solved implicitly using a tridiagonal matrix solver. Melting at the top surface, along with melting and growth at the bottom surface, are a function of the net radiative and turbulent fluxes exchanged with the atmosphere and ocean. The shortwave albedo is a function of ice and snow thickness and temperature in each of two radiative bands, visible and near IR. Turbulent exchange with the atmosphere follows Large (1998), while the ice–ocean heat flux is based on McPhee (1992). The top-surface fluxes depend on the new-time surface temperature and are computed within the sea ice model for each ice category.

The linear remapping scheme of Lipscomb (2001) is used to transport ice between neighboring categories as it grows and melts. Each category has a fractional area a, which is unchanged by vertical thermodynamic processes, and a thickness h, which does change. Thermodynamic growth and melting can be thought of as a Lagrangian motion of ice categories in thickness space, during which the area (but not volume) of ice in each category is conserved. Linear remapping is less diffusive than the simpler scheme of Hibler (1980), which fixes the ice thickness in each category.

The sea ice receives from the ocean a potential heat flux for freezing or melting ice. When this potential is positive, frazil ice grows in open water and then is merged with the ice in the thinnest category. When the potential is negative, heat is available to the ice and is partitioned between basal and lateral heat exchange. The exchange results in a lateral melt rate, which depends on the ice–ocean temperature difference and a prescribed mean floe diameter following Steele (1992). The basal ocean heat exchange is balanced by the conductive heat flux at the ice base and the latent heat exchange that results from basal ice melt or growth.

Velocities are computed from the sea ice momentum equation following Hunke and Dukowicz (1997), as updated by Hunke (2001) and Hunke and Dukowicz (2002). The force balance includes wind stress, ocean stress, internal ice stress, the Coriolis force, and a stress associated with sea surface tilt. The internal ice stress is derived from the elastic–viscous–plastic (EVP) rheology, a generalization of the viscous–plastic (VP) rheology of Hibler (1979). The ice flows plastically under typical stresses but is treated as a viscous fluid when strain rates are small and the ice is nearly rigid. An elastic term is added to improve the response to high-frequency forcing and to allow explicit time stepping. The ice diverges readily, as desired, but resists convergence and shearing. Each thickness category is transported by the same velocity field.

The ice is transported horizontally using the incremental remapping scheme of Lipscomb and Hunke (2004), which follows the work of Dukowicz and Baumgardner (2000). The ice area and various tracer fields (thickness, enthalpy, and surface temperature) are constructed in each grid cell as linear functions of x and y. The velocities are projected backward from cell corners to define departure regions, and the various conserved quantities (area, volume, and internal energy) are integrated over departure regions to determine the transports across each cell edge. Remapping is conservative and is second-order accurate in space, except where the field gradients are limited to preserve monotonicity. This scheme is relatively efficient for transporting many fields because much of the work is geometrical and is done only once per time step, instead of being repeated for each field.

Mechanical redistribution is parameterized following Rothrock (1975), Thorndike et al. (1975), and Hibler (1980). Divergent motion results in open water formation, whereas convergence causes ice ridging and rafting, and shearing causes both open water and ridges to form. In ridging, thin ice is replaced by a smaller area of thicker ice, conserving volume and internal energy. The thinnest 15% of the grid cell is available to participate in ridging and results in a distribution of ridged ice (Hibler 1980). During ridging, any snow that is present on the ice that undergoes ridging is assumed to fall into the ocean. This modifies the ocean heat and freshwater content in a conservative manner. The ice strength used by the EVP scheme when an ITD is present is computed as a function of the increase of potential energy under mechanical deformation (Rothrock 1975). This results in an ice strength that depends on the subgrid-scale distribution of ice thickness.

Following Bitz et al. (2001) and Lipscomb (2001), there are five ice thickness categories and an open water category in the standard CSIM configuration. The prognostic variables for each category are the fractional area, ice thickness, snow thickness, surface temperature, ice temperature/enthalpy (in each of four layers), and snow temperature/enthalpy. The category boundaries are computed from a formula that gives closer spacing for thinner categories. For the standard setup the lower category boundaries are 0, 0.65, 1.39, 2.47, and 4.60 m. The number of categories can be changed by the user, yielding a different set of boundaries. In single-category simulations, transport in thickness space is unnecessary, and ridging simply decreases the ice area while increasing the thickness. The ice strength

TABLE 1. Model simulations used in this study.

Run name	Configuration	Number of ice categories	CO_2 conditions	Length (yr)	Tuning
C_ITD	Coupled	5	Present day	100	None
C_1CAT	Coupled	1	Present day	100	None
S_ITD	SOM	5	Present day	30	None
S_1CAT	SOM	1	Present day	30	None
S_lCATt	SOM	1	Present day	30	Albedo
S_ITD_CO2	SOM	5	$2XCO_2$	30	None
S_1CAT_CO2	SOM	1	$2XCO_2$	30	None
S_1CATt_CO2	SOM	1	$2XCO_2$	30	Albedo

of a single category is computed following Hibler (1979) as a function of thickness and open water area, since the multicategory parameterization gives excessive strengths in this case.

b. Experimental design

To examine the effects of the ITD on the climate of CCSM3, a number of integrations will be compared (Table 1). All of these runs use the T42-gx1 resolution, which is approximately 2.875° resolution for the atmosphere and an average of less than 1° resolution for the ocean and sea ice. Although a number of improvements in the sea ice simulation (see section 3c) are present with the higher T85-gx1 grid, the coarser resolution model is used for the ITD sensitivity integrations because of the reduced computational expense. The simulations analyzed include both fully coupled runs and runs with a coupled atmosphere–land–ice slab ocean model (SOM).

For the coupled simulations we compare century long control integrations with and without an ITD. These simulations were run from a quasi-equilibrated climate state, and were branched off the CCSM3 control integration that had run for 400 yr. They will be referred to as C_ITD and C_1CAT. The C_ITD simulation is the T42-gx1 control run and uses five ice categories and a single open water category as discussed above. The C_1CAT simulation includes a single ice and single open water category. It uses the Hibler (1979) ice strength formulation. These runs are compared to examine the influence of the ITD on the coupled climate state and variability in the climate system. Averages over the last 50 yr (year 450–499) are used for these comparisons.

To examine the influence of the ITD on climate feedbacks, additional SOM runs were performed. These simulations use the full atmosphere–land–sea ice model, but a single-layer slab ocean model, which has specified ocean heat transports. This SOM model configuration is different from that discussed elsewhere in this issue (e.g., Collins et al. 2006b) in that it uses the full dynamic–thermodynamic sea ice model discussed above. The slab ocean model component represents a 50-m-deep heat reservoir in which the temperature evolves due to surface heat exchange and a specified annually periodic ocean "qflux," which represents lateral and vertical ocean exchange. The ocean heat transports (qflux) were obtained from the control climate coupled integration. The simulated climatology of the SOM configuration is similar to that of the fully coupled model, although the Southern Hemisphere sea ice is considerably thinner in the SOM runs. This SOM configuration allows the model to equilibrate quickly and was used to investigate the influence of the ITD on climate feedbacks because of computational considerations. However, it is important to note that the SOM runs only allow for very limited ocean feedbacks and neglect any influence of the ITD or climate change on ocean circulation and heat transports. This has some important consequences as noted below. SOM integrations were performed for present day and $2XCO_2$ conditions, with and without an ITD. The $2XCO_2$ conditions provide a perturbed forcing that allows us to assess the influence of the ITD on the polar climate response and feedbacks. As such, we will not extensively analyze the climate change itself in these simulations but instead will focus on simulated sea ice related feedbacks. These are referred to as S_ITD, S_1CAT for the present day runs and S_ITD_CO2 and S_1CAT_CO2 for the $2XCO_2$ runs.

Simulating the ITD has a considerable effect on the mean present day climate state as discussed below. Some aspects of the mean state influence the simulated response to increased CO_2 levels (e.g., Holland and Bitz 2003), making it difficult to attribute differences in the $2XCO_2$ simulations to feedbacks that depend directly on the ITD physics and not the influence of the ITD on the mean state. To isolate the ITD influences, an additional set of tuned SOM runs were performed. These simulations have a single ice and single open

water category as in the S_1CAT and S_1CAT_CO2 runs, but the surface ice albedo has been increased by 0.13 to obtain a hemispheric ice volume, which is more similar to the S_ITD runs. These runs are referred to as S_1CATt and S_1CATt_CO2, where the additional "t" stands for "tuned" integration. All of the SOM simulations were integrated for 30 yr, at which point they had essentially equilibrated. Conditions were averaged over the last 10 yr of these integrations for the analysis in sections 3 and 4.

3. Sea ice simulation of the CCSM3 T42 control run

Here we present the CCSM3 sea ice simulation from the T42-gx1 control run. Years 450–499 are analyzed for consistency with single-category sensitivity runs discussed in section 4. Differences between the sea ice in the T42-gx1 and T85-gx1 CCSM3 control simulations are discussed.

a. Northern Hemisphere

Figure 1 shows seasonal averages of ice thickness over years 450–499 of the coupled control simulation (C_ITD). The thick solid line shows the 10% concentration taken from Special Sensor Microwave Imager (SSM/I) data (Cavalieri et al. 1997). As indicated by the 0.1-m contour, which gives a reasonable approximation to the ice extent, the Northern Hemisphere simulated extent agrees reasonably well with observations. However, the winter ice extent is too large in the Sea of Okhotsk and the Labrador Sea and too small in the Barents Sea as compared to observations. The Barents Sea bias is associated with anomalously high ocean heat transport to this region.

The mean annual cycle of the simulated Northern Hemisphere total ice area (Fig. 2) shows that wintertime monthly averages are larger than the observations because of the extensive ice cover in the Sea of Okhotsk and Labrador Sea. The summertime minimum ice area is considerably larger than the SSM/I data but agrees remarkably well with the Hadley Centre Sea Ice and SST (HadISST) data (OI.v2 1982–2001; Rayner et al. 2003). The HadISST product is a globally gridded dataset that incorporates a number of observations, including the SSM/I data. Although, the Northern Hemisphere ice extent (defined as the region with ice concentration larger than 0.15) is similar between the SSM/I and HadISST data (Rayner et al. 2003), HadISST has a smaller open water area within the pack and larger ice area because it corrects for a high open water bias in the SSM/I data that is related to surface melting.

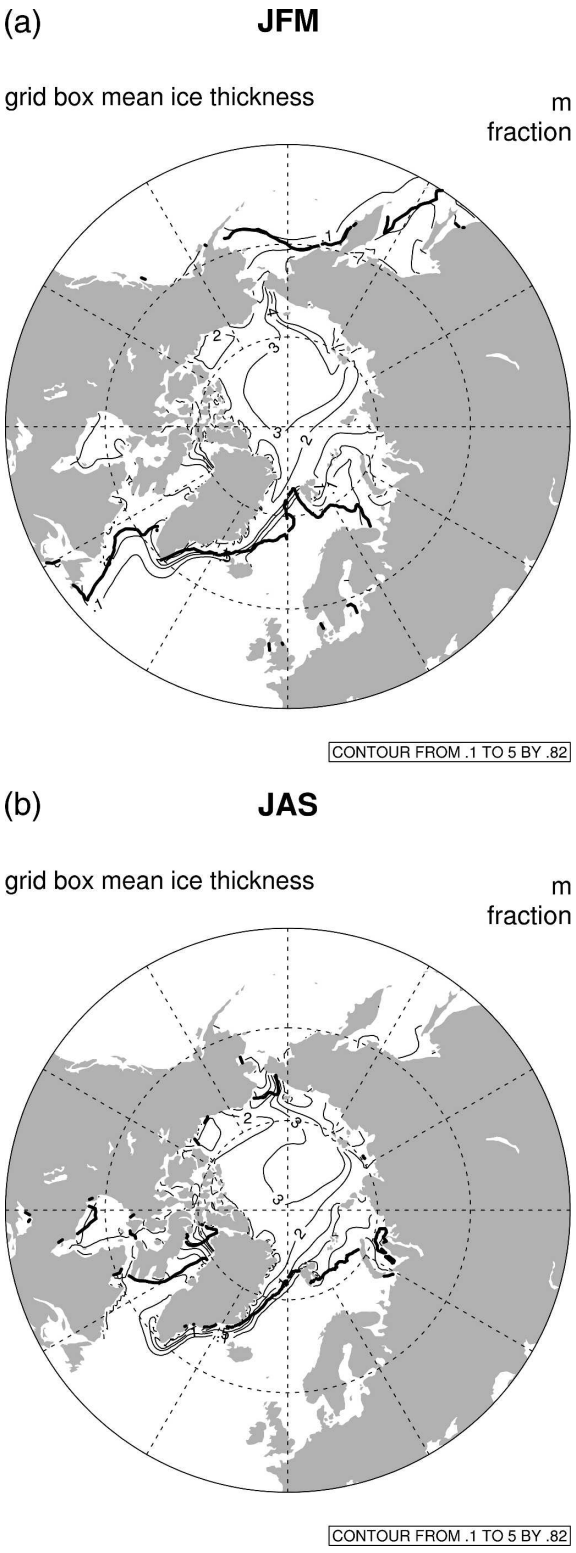

FIG. 1. Ice thickness averaged over years 450–499 of the coupled control simulation for (a) January–March and (b) June–September seasonal averages. Shown are the 0.1-, 0.5-, 1-, 2-, 3-, 4-, and 5-m contour intervals. The bold line shows the 10% contour interval from the SSM/I observations for 1979–99.

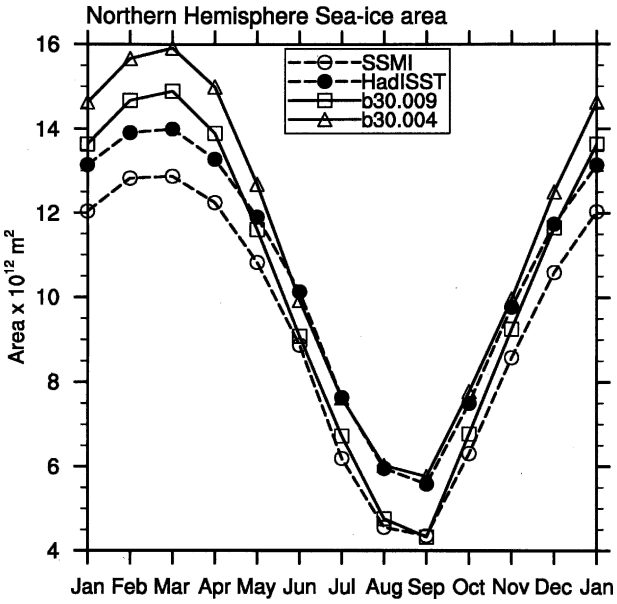

FIG. 2. Mean annual cycle of ice concentration from the model simulation and observations. The case name b30.004 represents the T42-gx1 simulation and the case name b30.009 represents the T85-gx1 simulation.

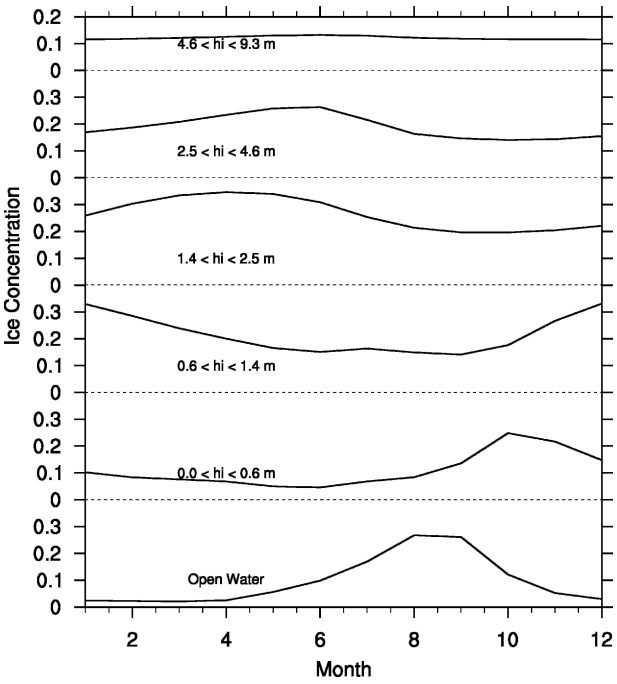

FIG. 3. The annual cycle of the ice thickness distribution from 80° to 90°N in the central Arctic. The fractional coverage in each ice category is shown.

The mean ice thickness in the central Arctic (Fig. 1) is about 3 m, which agrees well with the observed values of 2–3 m. Due in part to biases in the wind forcing, ice accumulates along the coast of the East Siberian Sea instead of against the Canadian Archipelago as observed. The influence of atmospheric resolution on this behavior is discussed in DeWeaver and Bitz (2006). In many aspects the ice velocity field in the T42-gx1 simulation looks quite reasonable and the ice volume flux through Fram Strait is 0.1 Sv, which compares well to observations (Vinje 2001).

The annual cycle of the ITD averaged from 80°–90°N (Fig. 3) indicates that a maximum open water fraction of approximately 25% occurs in August and September. This freezes over in October, resulting in a substantial increase in thin ice area. The ice continues to grow throughout the fall and winter, increasing the fractional area covered by thicker ice categories. The thickest ice category, which largely represents ridged ice, stays nearly constant throughout the year at approximately 10% fractional coverage. Qualitatively, the annual cycle of the ITD within the central Arctic agrees quite well with single-column model studies, which are forced with observed atmosphere and ocean conditions (e.g., Schramm et al. 1997; Holland et al. 1997).

b. Southern Hemisphere

Figure 4 shows the simulated seasonal climatological Southern Hemisphere ice thickness. The thick solid line shows the 10% concentration from SSM/I data. As indicated by the 0.1-m contour, the simulated ice is too extensive in the Atlantic and Indian Ocean sectors of the Southern Ocean. Although this bias is present throughout the year, the amplitude of the annual cycle of SH ice area simulated by the model is realistic (Fig. 5).

Observations of Antarctic sea ice indicate that much of the ice cover is less than 1-m thick with local maxima approaching 3 m in the Ross and Weddell Seas (e.g., Timmermann et al. 2004). Compared to observations, the simulated distribution of ice thickness around the continent (Fig. 4) is reasonable. However, the ice is biased thick especially on the eastern side of the Antarctic Peninsula, which exceeds 5 m in thickness. This is likely related to excessive ice convergence in this region. The thick Weddell Sea ice cover results in excessive equatorward ice transport, which influences the global hydrological cycle (Hack et al. 2006) and contributes to the large ice extent in this region.

The annual cycle of the ice thickness distribution averaged over the Atlantic sector of the Southern Ocean (from 60°W–20°E and poleward of 50°S; Fig. 6) clearly demonstrates the largely seasonal nature of the Antarctic sea ice, with maximum open water areas approaching 80% in the summer. This results in a large percentage of thin ice cover in the austral fall as this

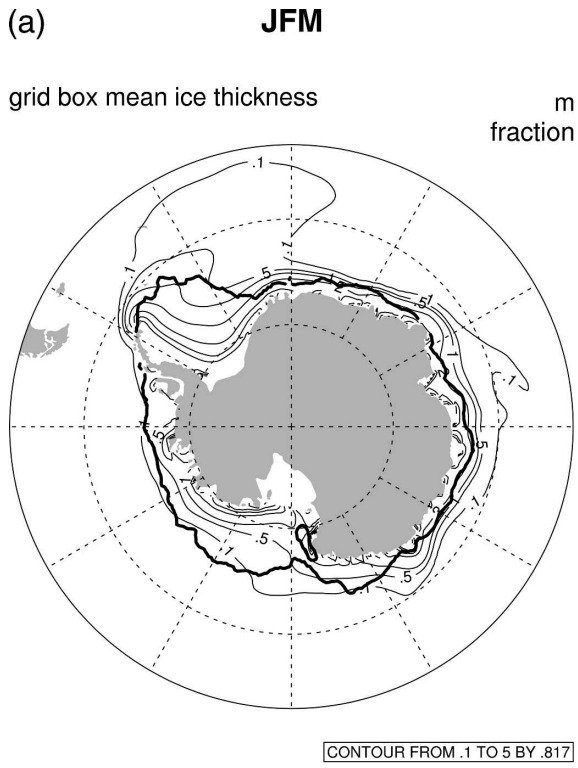

FIG. 4. As in Fig. 1 but for the Southern Hemisphere.

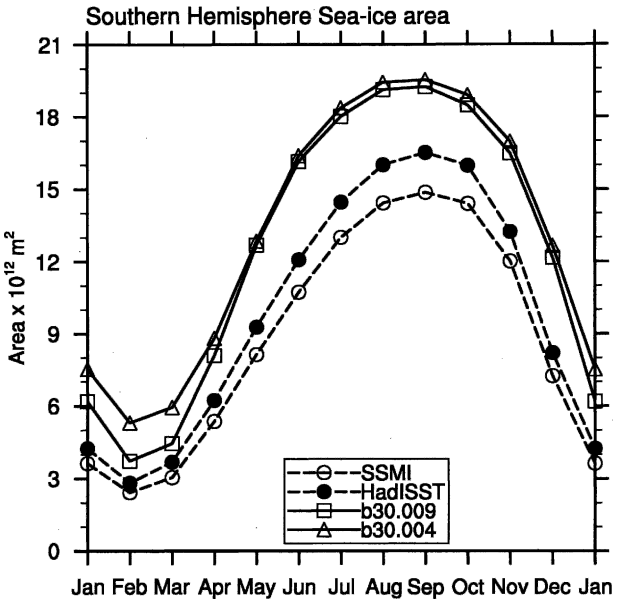

FIG. 5. The annual cycle of ice area in the Southern Hemisphere. The case name b30.004 represents the T42-gx1 simulation and the case name b30.009 represents the T85-gx1 simulation.

open water freezes over. The majority of the sea ice remains below 1.5 m in thickness throughout the year. However, the amount of ridged ice in the thickest category is excessive for the large region that encompasses

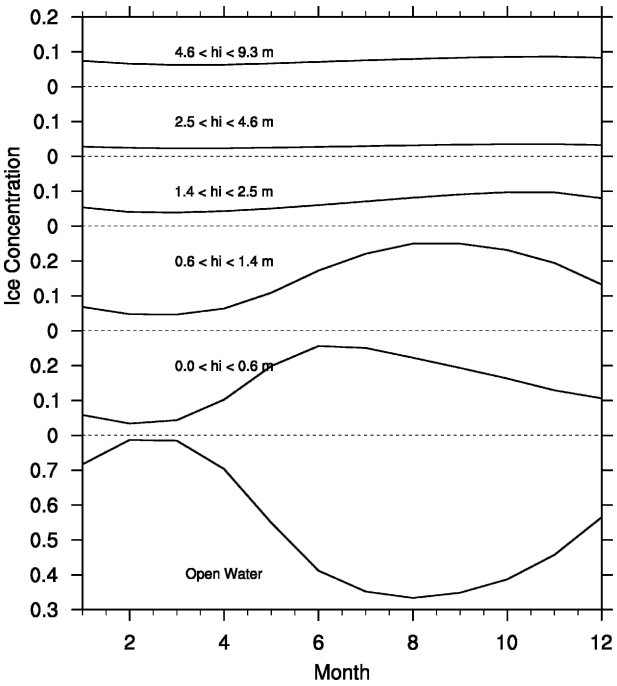

FIG. 6. The annual cycle of the ice thickness distribution in the Atlantic sector of the Southern Ocean.

this average. This is associated with the excessively thick sea ice along the Antarctic Peninsula.

c. *The T85-gx1 control simulation compared to the T42-gx1 control simulation*

While this paper focuses on simulations using the T42-gx1 model resolution, it is worth noting that a higher resolution CCSM model simulation is also available and has long control integrations as discussed by Collins et al. (2006a). This coupled control simulation differs from C_ITD in that the resolution of the atmosphere has been increased from the T42 (approximately 2.875°) to the T85 (approximately 1.4°) grid. Overall, the higher resolution simulation shows several changes, many of which are improvements, in the sea ice simulation. These include:

1) In the Northern Hemisphere, the ice extent has decreased in the Sea of Okhotsk and the Labrador Sea, although it is still too extensive in the winter as compared to observations (Fig. 2). There is still not enough ice in the Barents Sea.
2) The Arctic ice has thinned considerably in the T85 simulation, resulting in a mean ice thickness within the Arctic of 2.0 m compared to 2.75 m in the T42-gx1 run. This contributes to a smaller summer ice cover (Fig. 2) as the thinner ice is more easily melted away.
3) Thicker Arctic ice is accumulated against the Canadian Archipelago as observed. The reasons for this, including an analysis of the changes in Arctic atmospheric circulation, are discussed in DeWeaver and Bitz (2006).
4) While the Southern Hemisphere ice area is still too excessive, it has decreased (Fig. 5), particularly in the austral summer.
5) The ice along the Antarctic Peninsula has thinned considerably, but is still too thick.

4. Influence of the ITD on mean climate

Previous studies (e.g., Bitz et al. 2001; Holland et al. 2001) have found that resolving the ice thickness distribution increased the total sea ice volume and the amplitude of the sea ice annual cycle, resulted in warmer surface air temperatures in ice covered regions, and led to increased Arctic sea surface salinity. These studies used a coupled model system with an energy–moisture balance atmosphere with no atmospheric dynamical feedbacks. Our study extends this previous work with the use of a fully coupled general circulation model.

Here, we present results of the model sensitivity to simulating the ITD using two different model configurations (Table 1). These include fully coupled model simulations and atmosphere–sea ice slab ocean model simulations. Comparing results from these two configurations clarifies the role that ocean circulation plays in the coupled model response to an ITD.

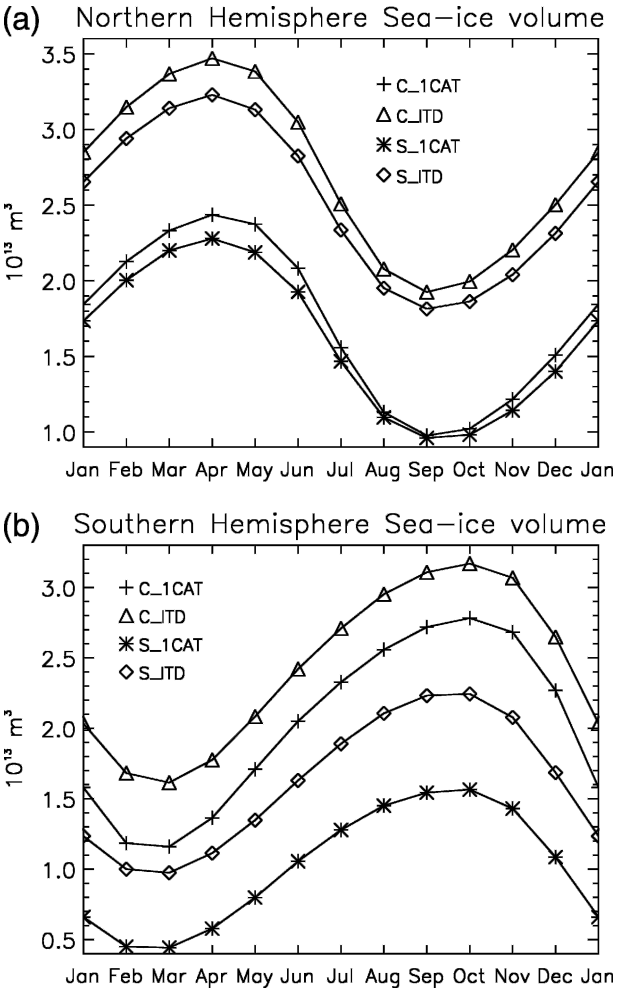

FIG. 7. The ice volume annual cycle for (a) the Northern Hemisphere and (b) the Southern Hemisphere.

The influence of the ITD in CCSM3 in both the fully coupled and SOM configurations generally agrees with the results from intermediate climate models in previous studies. The sea ice cover is thicker in both hemispheres with an ITD (Fig. 7) due to larger ice growth rates, particularly in regions of relatively thick sea ice. The increased thermodynamic source of ice is balanced by increased equatorward ice transport. The ultimate fate of this increased ice volume flux to low latitudes is dependent on the hemisphere and model configuration as discussed below.

In further agreement with previous studies, the surface air temperature (SAT) is warmer in the presence

of an ITD particularly over the perennial ice pack (Fig. 8). Although the ice is thicker in the ITD runs, resolving thin ice cover within the pack increases the sensible heat loss to the atmosphere. The SAT response is quite different in the coupled and SOM model configurations, with the coupled model having a much larger and more significant response, particularly in the Southern Hemisphere. In the coupled ITD run, larger ice growth rates and brine rejection enhance Southern Ocean convection resulting in a modified meridional overturning circulation (Fig. 9) and enhanced Antarctic bottom water production. A larger poleward Southern Ocean heat transport results, producing a considerably smaller Southern Ocean ice extent when the ITD is resolved. This allows more ocean–atmosphere heat exchange and a warmer atmosphere. As ocean heat transport is held fixed in the SOM integrations, this process is inactive and the simulated response to the ITD is much reduced.

The changes in surface conditions also modify the atmospheric circulation. These are most dramatic in the Southern Hemisphere of the coupled runs, where resolving the ITD results in higher sea level pressure (SLP) in high southern latitudes and lower SLP in southern midlatitudes (Fig. 10). This has a similar structure to the Southern Annular Mode (Thompson and Wallace 2000). The reduced SLP gradient results in weaker westerlies and reduces the equatorward Ekman ocean and ice transport. This contributes to the reduced sea ice extent in the coupled ITD simulation.

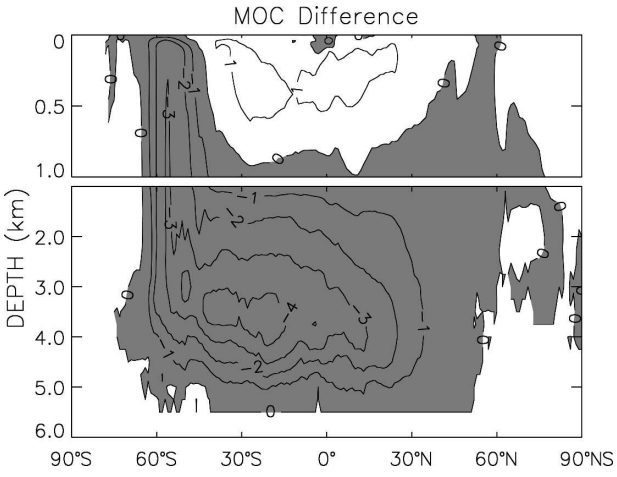

FIG. 9. Change in the meridional overturning circulation in response to the ITD for the fully coupled runs (C_ITD-C_1CAT). The contour interval is 1 Sv and negative values are shaded.

In the Northern Hemisphere, the SLP is not changed considerably in the coupled integrations. However, the SOM runs have increased SLP in the ITD simulation over the North Atlantic/Nordic seas, extending into northwestern Europe (not shown). This is a region of high SLP variability associated with the North Atlantic Oscillation (NAO) and it is not clear that the changes are significant and can be attributed to the different sea ice physics. Longer simulations or multiple ensembles of the SOM model, which were not feasible for this study, would be needed to determine if the Northern

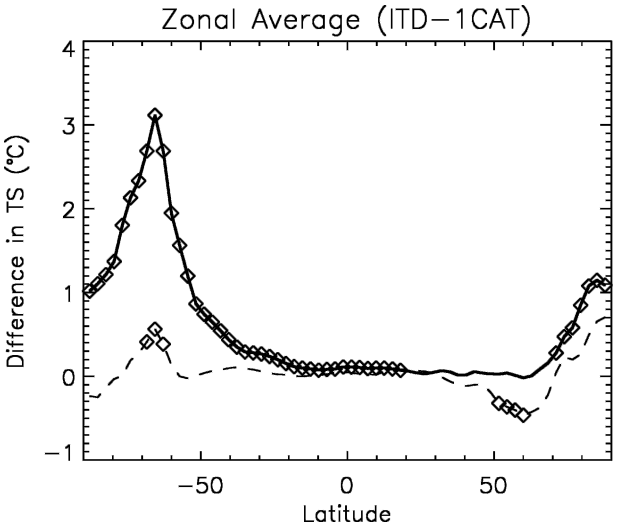

FIG. 8. The change in zonally averaged surface air temperature in simulations with an ITD minus simulations without an ITD. The solid line denotes the coupled model runs (C_ITD-C_1CAT) and the dashed run shows the SOM integrations (S_ITD-S_1CAT). Differences that are significant at the 99% level are marked with diamonds.

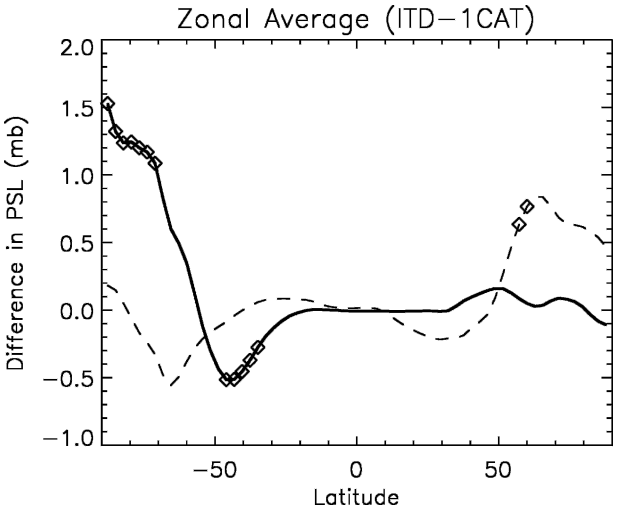

FIG. 10. The zonally averaged change in SLP (ITD-no ITD). The solid line denotes the coupled model runs (C_ITD-C_1CAT) and the dashed run shows the SOM integrations (S_ITD-S_1CAT). Differences that are significant at the 99% level are marked with diamonds.

Hemisphere SLP changes are robust or are instead associated with natural model atmospheric variability.

5. Influence of the ITD on simulated feedbacks

The ITD modifies ice–ocean–atmosphere heat and freshwater exchange and sea ice growth and melt rates with consequent influences on polar climate conditions. As many sea ice feedbacks are associated with changes in ice growth rates and open water formation, it is reasonable to expect that the ITD will influence these feedbacks. This has the potential to modify simulated climate sensitivity and polar amplification.

At transient $2XCO_2$ conditions, CCSM3 exhibits a maximum zonally averaged Arctic warming that is approximately 4.3 times the global average compared to 2–3 times the global average for most of the Coupled Model Intercomparison Project version 2 (CMIP2) models (Holland and Bitz 2003). There are likely a number of factors driving the high polar amplification in CCSM3 including changes in Arctic Ocean circulation (Bitz et al. 2006). Here we investigate whether the inclusion of an ITD might also contribute to the relatively high polar amplification in CCSM3 by modifying simulated sea ice–related feedbacks.

a. Surface albedo feedback

Arguably the most important positive sea ice feedback is that associated with changes in the surface albedo. Reductions in sea ice cover result in increased absorption of solar radiation, which acts to further reduce the sea ice cover. The efficiency by which an increased ice melt rate results in open water formation and a large change in surface albedo modifies the strength of this feedback. We hypothesize that the presence of an ITD, which resolves thin ice within the pack, should result in a stronger albedo feedback, as the thin ice categories are easily removed.

In examining the strength of the albedo feedback, we start with the classic definition of climate sensitivity (e.g., Houghton et al. 2001), where the change in equilibrium surface temperature (ΔT_{eq}) in response to a radiative forcing change (ΔF) is

$$\Delta T_{eq} = \lambda \Delta F. \tag{2}$$

The value λ is a climate sensitivity parameter that quantifies the radiative feedbacks. Accounting for changes in outgoing longwave radiation (F_{LW}) and incoming shortwave radiation (F_{SW}) results in

$$\lambda = \left(\frac{dF_{LW}}{dT} - \frac{dF_{SW}}{dT} \right)^{-1}, \tag{3}$$

where T is the surface air temperature. Following Hall (2004), we isolate the surface albedo feedback contribution to the climate sensitivity by examining the variation in the net incoming shortwave radiation with surface air temperature due to surface albedo (α) changes:

$$\left(\frac{\partial F_{SW}}{\partial T} \right)_{SAF} = \frac{\partial F_{SW}}{\partial \alpha} \left(\frac{d\alpha}{dT} \right). \tag{4}$$

As we are interested in the ITD influence on the surface albedo feedback, we focus on the relationship between surface albedo and surface air temperature (the $d\alpha/dT$ term).

Figure 11 shows the change in surface albedo per change in SAT ($d\alpha/dT$) for ice-covered regions as a function of the initial summer ice thickness for the SOM $2XCO_2$ minus SOM present day integrations. The Northern and Southern Hemispheres are shown separately. To remove seasonal ice cover from our analysis, only regions with initial September (March) ice thicker than 0.5 m for the Northern (Southern) Hemisphere were considered. All the integrations show a larger reduction in albedo on a $°C^{-1}$ basis for thinner ice cover, as this ice is more easily removed. Additionally, for ice of the same thickness, the ITD simulation typically has a larger reduction in albedo on a $°C^{-1}$ basis compared to the single category simulations. This indicates a stronger local surface albedo feedback for ice of the same initial thickness.

The ice is considerably thicker when an ITD is included. This may affect the albedo feedback analysis. Therefore, an additional simulation (S_1CATt) was performed in which the bare ice albedo was increased by 0.13 in the 1CAT model to give a mean hemispheric ice thickness that is similar to the ITD case. Results from this simulation (Fig. 11) indicate that the S_1CATt and S_1CAT simulations obtain a similar change in albedo per change in SAT for ice of the same initial thickness and both of them have a considerably reduced response compared to the ITD run. The similar behavior in the single category simulations suggests that this response is robust.

b. Ice thickness–ice growth rate feedback

Sea ice–related feedbacks can also modify the sea ice thickness response to climate perturbations. Many of these feedbacks are associated with changes in ice growth rates under perturbed climate conditions. Ice formation results from a heat loss from the ice–ocean column to the overlying atmosphere. Thus, a change in ice growth rate represents a redistribution of energy within the system and a modified atmospheric energy

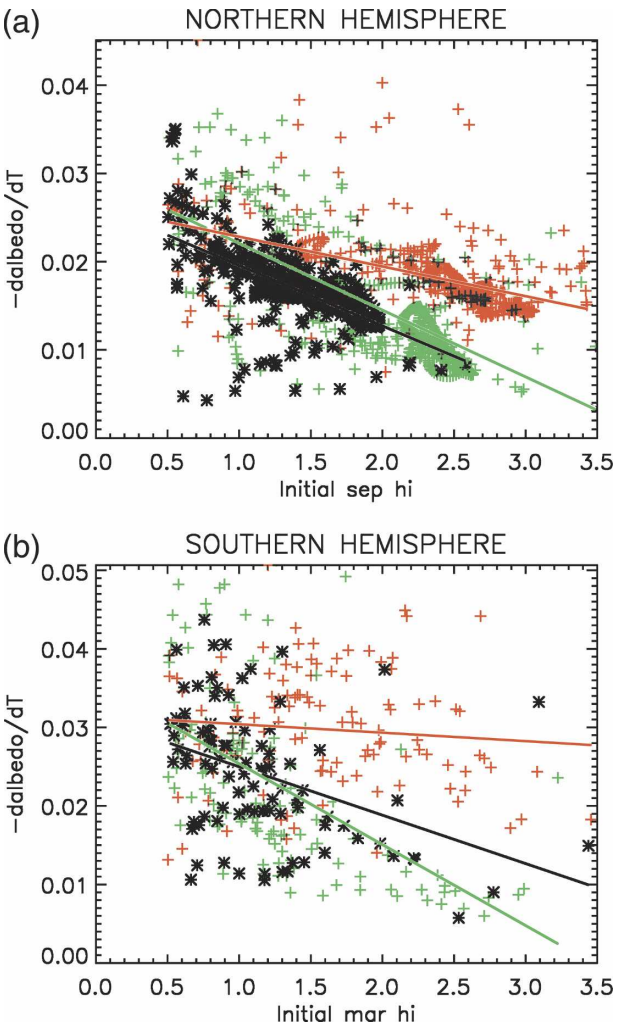

FIG. 11. The change in surface albedo per surface air temperature change at $2XCO_2$ conditions {e.g., [α(2XCO2)-α(control)]/[T(2XCO2)-T(control)]} as a function of initial summer minimum sea ice thickness for (a) the Northern Hemisphere and (b) the Southern Hemisphere. The September (March) average ice thickness is used to represent the summer minimum for the Northern (Southern) Hemisphere. Regions with initial sea ice thinner than 0.5 m are not used in this analysis. Values shown are for the ITD simulation (red), 1CAT simulation (black), and 1CATt simulation (green).

budget. In contrast to changes in the surface albedo, changes in ice growth rates do not necessarily modify the total energy in the system. As such, while changes in ice growth rates influence the ice thickness response to climate perturbations, they do not necessarily modify the surface air temperature response.

Sea ice growth rates depend nonlinearly on the reciprocal of ice thickness so that as ice thins, growth rates increase, resulting in a negative feedback on ice thickness (e.g., Bitz and Roe 2004; L'Heveder and Houssais 2001). This feedback is stronger for thin ice cover. As the ITD resolves thin ice within the pack, the mean ice growth rates increase, resulting in a thicker control climate sea ice cover. This may also influence the strength of the negative ice thickness–ice growth rate feedback and hence the ice thickness response to climate perturbations.

Bitz and Roe (2004) discuss the thermodynamics of the ice thickness–ice growth rate feedback. When ice dynamics is neglected, the equilibrium ice thickness is determined by the balance of ice growth and melt. By analogy to the climate sensitivity definition (section 5a), the change in equilibrium ice thickness (Δh_{eq}) in response to a forcing perturbation (ΔF) can be expressed as

$$\Delta h_{eq} = \lambda_h \Delta F \tag{5}$$

(Bitz and Roe 2004), where λ_h is a thickness sensitivity parameter that quantifies the ice thickness feedbacks. Accounting for the thickness dependence of ice growth and melt, but neglecting ice dynamics, results in

$$\lambda_h = \left(\frac{\partial G}{\partial h} - \frac{\partial M}{\partial h}\right)^{-1}\left(\frac{\partial G}{\partial F} - \frac{\partial M}{\partial F}\right), \tag{6}$$

where G is the ice growth rate and M is the ice melt rate. As we are interested in the influence of the ITD on the ice thickness–ice growth rate feedback, we focus here on the $(\partial G/\partial h)^{-1}$ term. The melt rate (M) only weakly depends on ice thickness, which results from albedo changes that were implicitly considered in the albedo feedback analysis in section 5a.

As indicated by Eq. (6), the change in equilibrium ice thickness in response to a forcing perturbation increases with the reciprocal of the change in ice growth rate (G) per change in ice thickness (h), or with $(\partial G/\partial h)^{-1}$. Because $(\partial G/\partial h)^{-1}$ is a strong function of h, the thinning in response to increasing CO_2 is also a strong function of h. Here we assess the relationship between ice growth rates and ice thickness in the SOM climate change integrations. We focus on Arctic sea ice conditions as the large ocean heat fluxes and seasonal ice cover in the Southern Hemisphere complicate the picture. However, an analysis was performed for the Southern Hemisphere (not shown) and the results are generally consistent with those presented here for the Arctic.

The change in ice growth rate per change in ice thickness ($\partial G/\partial h$) from the $2XCO_2$ SOM integrations for grid cells with an initial ice thickness greater than 0.5 m is shown in Fig. 12. In these climate change simulations, the growth rates are influenced by the changing ice thickness in combination with changes in the forcing associated with the CO_2 increase and other feedback

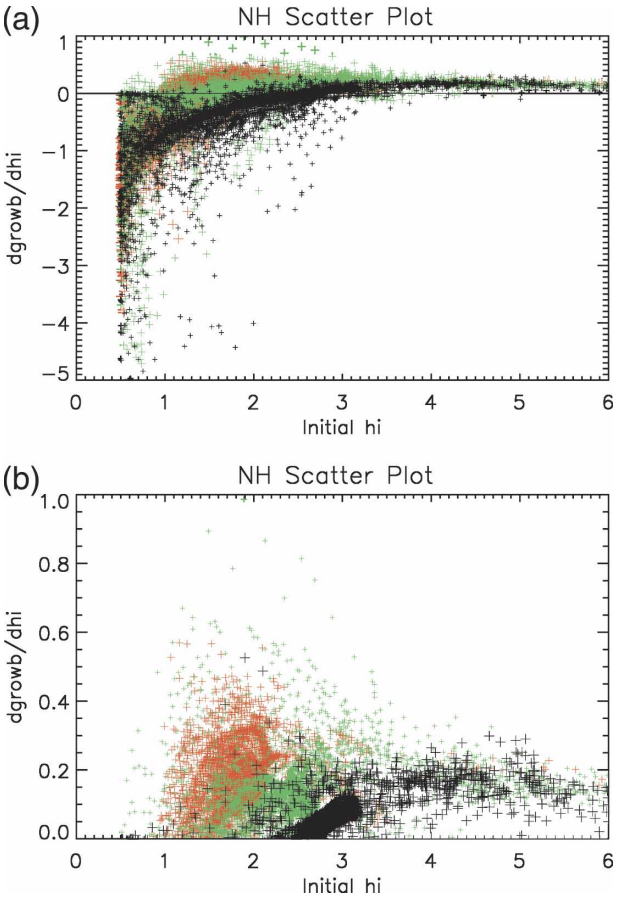

FIG. 12. The change in ice growth per decrease in ice thickness at $2XCO_2$ conditions as a function of the initial ice thickness. Shown are results from the Northern Hemisphere for the SOM integrations, including S_ITD (black), S_1CAT (red), and S_1CATt (green). (a) All points and (b) points that have an increased growth rate at $2XCO_2$ conditions.

mechanisms. In general, for relatively thin ice, the growth rate decreases as the ice thins, due to the increased radiative forcing and mechanisms such as the ice–albedo feedback. This decrease in ice growth rate is larger for the ITD simulation possibly because of the enhanced albedo feedback indicated by the analysis in section 5a.

For thicker ice cover, increased growth rates do occur at the $2XCO_2$ conditions. On a grid cell basis for ice of the same initial thickness (Fig. 12b), the single category simulations typically have a larger increase in ice growth rates than the ITD run. On the Arctic average, this results in a 7% (13%) increase in ice growth rates for the single category (tuned) integration at $2XCO_2$ conditions. In contrast, the ITD simulation has a net decrease in Arctic ice growth of approximately 1%. This suggests that the stabilizing ice thickness–ice growth rate feedback is weaker in the ITD simulation. As the ITD resolves regions of thin rapidly growing ice cover within the pack ice under present day conditions, a smaller fraction of slow-growing thick ice can be replaced by thin ice as the climate warms. Because of the nonlinear nature of the ice thickness–ice growth rate relationship, this causes a smaller increase in ice growth rates as the mean ice thickness is reduced. This should result in a larger change in ice thickness for the ITD run at $2XCO_2$ conditions as the growth rates have a weaker stabilizing effect on ice thickness.

Although the relationship between ice thickness and ice growth rate acts as a negative feedback on the thickness of the ice, this does not necessarily translate into a negative feedback on surface air temperature. The net surface heat flux to the atmosphere depends on ice formation, such that during ice growth, heat is lost from the ocean/ice column either through leads or at the ice surface and gained by the atmosphere. Thus, increased ice formation represents an increased atmospheric heat flux. Whether this increases the heat flux on the annual average depends on how the modified ice growth rate is balanced by ice melting (which represents a sink of heat from the atmosphere and/or ocean) and ice export. If increased growth is balanced by increased export, an increase in the source of heat to the Arctic atmosphere can result. As shown below (section 5d), these considerations can be important for assessing the net influence of the ITD on climate sensitivity.

c. *Ice thickness–ice strength feedback*

Previous ice-only model experiments have suggested that the ice thickness–ice strength relationship represents a negative feedback such that ice dynamics stabilizes the ice pack (e.g., Hibler 1984; Holland et al. 1993). Because thinner ice is weaker and less resistant to convergence, if a region experiences thermodynamic thinning, increased convergence can counteract the thermodynamic effects. This acts as a negative feedback on ice thickness.

As discussed in section 2, the ice strength is determined differently in the ITD and single category simulations. This can modify the ice thickness–ice strength relationship. Figure 13 shows the ice strength as a function of ice thickness for the coupled and SOM model control simulations. In the single category runs, a simple linear approximation between ice thickness and ice strength is apparent and the two are correlated at greater than 0.9 in both hemispheres. For the ITD simulations, more scatter in ice strength occurs for a given ice thickness. This is to be expected as the ice strength is determined from the thickness distribution,

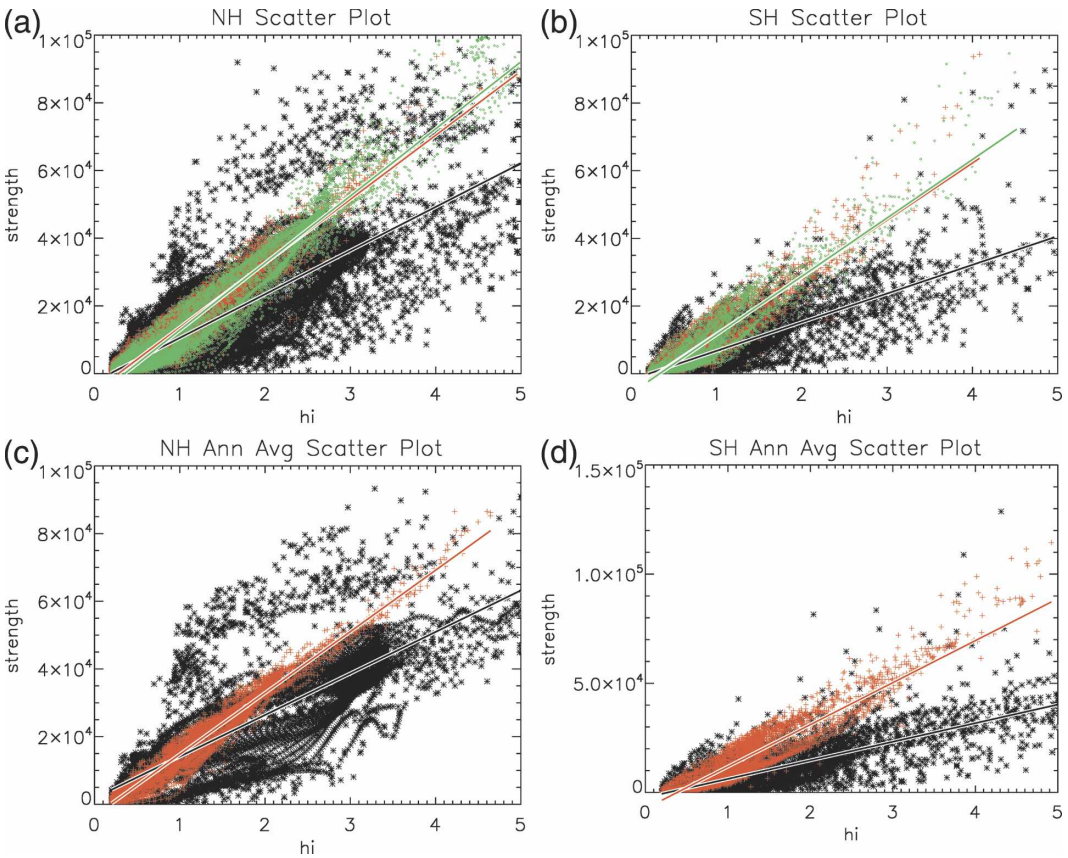

FIG. 13. Scatterplots of the annual average ice strength as a function of annual average ice thickness for SOM and coupled model control integrations for the Northern and Southern Hemispheres. Analysis is shown for (a) SOM integrations in the Northern Hemisphere, (b) SOM integrations in the Southern Hemisphere, (c) coupled integrations in the Northern Hemisphere, and (d) coupled integrations in the Southern Hemisphere. In (a) and (b), the black points denote the S_ITD simulation, the red points represent the S_1CAT run, and the green points represent the S_1CATt run. In (c) and (d) the black points represent the C_ITD run and the red points represent the C_1CAT run. The linear fit is shown on the plots as a solid line in the corresponding color.

which can differ for a given mean thickness. However, a linear relationship still quite accurately captures the ice thickness–ice strength relationship and the two are correlated at approximately 0.8 in all the ITD runs in both hemispheres.

The ITD simulations generally obtain a smaller ice strength for a given ice thickness indicating that the ice pack is less resistant to convergence. This could contribute to the thicker ice that is simulated under present day climate conditions when an ITD is used. Additionally, the change in ice strength per change in ice thickness is smaller for the ITD runs. This is confirmed by the SOM integrations that, for ice of the same initial thickness, show a smaller change in ice strength at $2XCO_2$ conditions for the multicategory runs (not shown). This suggests that the negative ice thickness–ice strength feedback is reduced in the ITD simulations because, when the ice thins, a smaller reduction in ice strength (and potential increase in ice convergence) occurs. This should result in larger ice thickness changes in the ITD simulations.

d. Overall effects

The net impact of the ITD on the simulation of variability and climate change results from an interplay of its relative effects on multiple feedbacks, including those mentioned here. Our results indicate that the ITD enhances the surface albedo feedback. Additionally, it reduces the stabilizing feedbacks on ice thickness associated with the ice thickness–ice strength relationship and the ice thickness–ice growth rate relationship.

Variance is damped (amplified) by strong negative (positive) feedbacks. Based on our analysis, the ITD should increase the simulated response of the ice thickness to climate perturbations. In the present day coupled model simulations, the ice thickness in both

TABLE 2. Hemispheric ice thickness in meters in the SOM integrations.

	Northern Hemisphere		Southern Hemisphere	
Run name	Initial h	Δh at $2XCO_2$	Initial h	Δh at $2XCO_2$
S_ITD	1.35	0.82	0.67	0.22
S_1CAT	0.93	0.46	0.47	0.12
S_1CATt	1.41	0.68	0.59	0.17

TABLE 3. Influence of the ITD on the simulated climate system as indicated by this study.

Mean climate	Feedbacks
Increased ice growth rates	Stronger albedo feedback
Thicker ice cover	
Warmer air temperatures in the presence of perennial sea ice	Weaker ice thickness–ice growth rate feedback
Increased brine rejection and consequent ocean circulation changes	Weaker ice thickness–ice strength feedback

hemispheres is considerably more variable in the ITD simulation (C_ITD) as compared to the single-category run (C_1CAT). However, the ice is also much thicker in the ITD integration, making it difficult to isolate the influence of the ITD versus the influence of the different mean conditions. For ice of similar mean thickness, the ITD simulation has a somewhat higher ice thickness standard deviation, suggesting that the ITD is in part responsible for some of the increase in ice thickness variability. However, the increased ice thickness variance in the ITD simulation does not translate into increased variability in surface atmospheric conditions, such as the zonally averaged surface air temperature.

The influence of the ITD on simulated sea ice feedbacks should also increase the sea ice thickness response under a climate warming scenario. The ITD simulations show a larger decrease in ice thickness compared to the single category runs for ice with the same initial thickness. Linearly regressing the change in ice thickness on the initial thickness, we find that at $2XCO_2$ conditions, the S_ITD simulation shows a decrease of 78% (47%) of its initial thickness, whereas S_1CAT and S_1CATt show a decrease of 66% (35%) and 64% (41%), respectively, for the Northern (Southern) Hemisphere. This indicates a stronger net feedback on the sea ice thickness in the ITD simulation. On the hemispheric average, this results in a larger sea ice thickness response in the S_ITD simulation as compared to the single category runs (Table 2).

However, this does not translate into larger surface warming in this simulation and the polar amplification in the CCSM3 SOM integrations with and without an ITD is quite similar and is slightly enhanced in the single category tuned simulation. The reasons for this are complex and involve small changes in multiple fluxes. The feedbacks discussed above influence these changes but are not the sole determinants. There also appear to be differences in, for example, cloud-cover changes and downwelling longwave radiation, which modify the simulated response. In this study, we have only considered feedbacks directly associated with the sea ice state and have not examined feedbacks associated with changes in things like polar clouds. These may compensate for the enhanced positive albedo feedback that is present with the ITD. Additionally, as discussed above, feedbacks that influence and stabilize sea ice thickness, such as the ice growth rate and ice strength feedbacks, do not necessarily translate into negative feedbacks on the surface air temperature as they represent a redistribution of heat within the ice–ocean–atmosphere system as opposed to a change in the heat within the system.

6. Discussion and conclusions

We have presented the sea ice model simulation of the CCSM3 and have discussed the influence of the subgrid-scale ice thickness distribution (ITD) on simulated mean climate conditions and sea ice related feedbacks. In general, the CCSM3 sea ice model simulation is quite good and reasonably captures the mean conditions and annual cycle of the sea ice area and thickness. However, in the T42-gx1 control simulation, there are some notable biases. For the Northern Hemisphere, these include relatively extensive winter ice cover in the Labrador Sea and North Pacific, too little ice cover in the Barents Sea, and an unrealistic Arctic ice thickness pattern, which has relatively thick ice along the Siberian coast and relatively thin ice along the Canadian Arctic Archipelago. In the Southern Hemisphere, the sea ice is too extensive in the Atlantic and Indian Ocean sectors and excessively thick in the Weddell Sea, particularly along the Antarctic Peninsula. Many of these biases are improved in the higher resolution T85-gx1 model simulation.

We assessed the influence of the ITD on simulated climate using both fully coupled century-long integrations and atmosphere–land–sea ice–slab ocean model (SOM) integrations. The primary results are summarized in Table 3. Consistent with previous studies with simpler model systems, the inclusion of an ITD parameterization increased the ice growth rates, resulted in thicker sea ice, and increased the surface air temperature in regions of perennial ice cover. Ocean circulation

and heat transport, particularly in the Southern Hemisphere, were modified by the ITD due to increased ice growth and brine rejection close to the Antarctic continent driving enhanced deep water formation. Atmosphere circulation changes were also associated with the presence of the subgrid-scale ITD, most notably in the Southern Hemisphere.

Our analysis of the simulated response to climate perturbations shows that the ITD also influences sea ice–related feedbacks. The different mean climate conditions that occur when an ITD is used can influence these simulated feedbacks. To isolate the ITD influence on the feedbacks from the mean climate influence, we have considered feedback relationships at $2XCO_2$ conditions as a function of the initial ice thickness. Additionally, we have used a tuned model integration in which the ITD and single category simulations have a more similar mean climate. The analysis is consistent between the tuned and untuned model simulations, indicating that we are capturing the ITD influence on the simulated feedbacks.

The influence of the ITD has been considered for the surface albedo feedback, the ice thickness–ice growth rate feedback, and the feedback associated with the ice thickness–ice strength relationship. We find that

1) The ITD enhances the positive surface albedo feedback. This occurs as the resolved thin ice cover present with an ITD is more easily melted away resulting in larger albedo changes for ice of the same mean thickness.
2) The ITD reduces the strength of the negative ice thickness–ice growth rate feedback. As the ITD resolves regions of thin rapidly growing ice cover within the pack ice under present day conditions, a smaller fraction of slow-growing thick ice can be replaced by thin ice as the climate warms. Because of the nonlinear nature of the ice thickness–ice growth rate relationship, this causes a smaller increase in ice growth rates as the mean ice thickness is reduced and results in a weaker negative feedback on ice thickness.
3) The ITD reduces the strength of the negative ice thickness–ice strength feedback. For ice of the same mean thickness, the ITD run has generally lower ice strength and a smaller increase in ice strength per ice thickness change. Thus a perturbation to the ice thickness results in a relatively small change in ice strength compared to the single category runs, allowing for a smaller change in ice convergence. Changes in dynamical ice thickening are then less able to counteract the initial ice thickness perturbation and a weaker negative feedback on ice thickness results. However, it should be noted that this result could be modified based on the parameters used in the ice strength formulation.

The net result from this feedback analysis is that the inclusion of an ITD should enhance the sea ice thickness response to external perturbations. Both the natural variability of the coupled model and climate change experiments with the atmosphere–land–sea ice slab ocean model do exhibit larger changes in sea ice thickness for the ITD runs. However, this does not necessarily translate into a larger surface air temperature response and the zonally averaged change in surface air temperature in $2XCO_2$ SOM integrations are quite similar regardless of the inclusion of an ITD. While changes in the strength of the surface albedo feedback modify the heat within the system and will influence the surface air temperature response, changes in the ice thickness–ice growth rate and ice thickness–ice strength relationships are feedbacks on ice thickness. A different ice thickness response to climate perturbations is associated with a change in the distribution of heat within the ice–ocean–atmosphere system but not necessarily a change in the total heat within the system. Additionally, other feedbacks not considered in this study, such as those associated with clouds, will influence the surface air temperature response.

It is worth noting, that in the climate change simulations, we have only considered equilibrated SOM model experiments at $2XCO_2$ conditions. However, the ITD is also likely to influence ice–ocean feedbacks not represented in these SOM integrations. For example, as discussed by Bitz et al. (2006), changes in Arctic ice growth rates in a climate change simulation influence and increase ocean heat transport into the Arctic and likely contribute to polar amplification. As the ITD is important for ice growth rates and the ice growth rate response to climate change, feedbacks of this type will likely be modified by the presence of an ITD. Additionally, the interplay of various feedbacks and their net effect on climate simulations evolves over transient climate simulations, which we have not considered in looking at the equilibrated SOM response.

Acknowledgments. Computational facilities have been provided by the National Center for Atmospheric Research (NCAR). Additional coupled sensitivity model integrations were performed by CRIEPI using the Earth Simulator through the international research consortium of CRIEPI, NCAR, and LANL under the Project for Sustainable Coexistence of Human Nature and the Earth of the Japanese Ministry of Education, Culture, Sports, Science and Technology. We thank Dr.

Peter Gent, Dr. John Walsh, and an anonymous reviewer for valuable comments on this manuscript. Additionally, we are grateful to the community of scientists who have contributed to the development of the CCSM3 model. This research was funded in part by a grant from the NSF Office of Polar Programs through the SHEBA phase 3 program to M. M. Holland. J. L. Schramm was supported by an NSF grant from the Office of Polar Programs made available through the NSF cooperative agreement to NCAR (NSF01). C. M. Bitz was supported by NSF ATM0304662.

REFERENCES

Bitz, C. M., and W. H. Lipscomb, 1999: An energy-conserving thermodynamic model of sea ice. *J. Geophys. Res.,* **104,** 15 669–15 677.

——, and G. H. Roe, 2004: A mechanism for the high rate of sea ice thinning in the Arctic Ocean. *J. Climate,* **17,** 3623–3632.

——, M. M. Holland, M. Eby, and A. J. Weaver, 2001: Simulating the ice-thickness distribution in a coupled climate model. *J. Geophys. Res.,* **106,** 2441–2463.

——, P. R. Gent, R. A. Woodgate, M. M. Holland, and R. Lindsay, 2006: The influence of sea ice on ocean heat uptake in response to increasing CO_2. *J. Climate,* **19,** 2437–2450.

Bjork, G., 1992: On the response of the equilibrium thickness distribution of sea ice to ice export, mechanical deformation and thermal forcing with application to the Arctic Ocean. *J. Geophys. Res.,* **97,** 11 287–11 298.

Briegleb, B. P., C. M. Bitz, E. C. Hunke, W. H. Lipscomb, M. M. Holland, J. L. Schramm, and R. E. Moritz, 2004: Scientific description of the sea ice component in the Community Climate System Model, Version Three. NCAR Tech. Note NCAR/TN-463+STR, 70 pp.

Cavalieri, D., C. L. Parkinson, P. Gloersen, and H. J. Zwally, 1997: Sea ice concentrations from Nimbus-7 SMMR and DMSP SSM/I passive microwave data, 1979–1999. National Snow and Ice Data Center, digital media and CD-ROM, updated 2004. [Available online at http://nsidc.org/data/nsidc-0051.html.]

Collins, W. D., and Coauthors, 2006a: The Community Climate System Model version 3 (CCSM3). *J. Climate,* **19,** 2122–2143.

——, and Coauthors, 2006b: The formulation and atmospheric simulation of the Community Atmosphere Model version 3 (CAM3). *J. Climate,* **19,** 2144–2161.

DeWeaver, E., and C. M. Bitz, 2006: Atmospheric circulation and its effect on Arctic sea ice in CCSM3 at medium and high resolutions. *J. Climate,* **19,** 2415–2436.

Dukowicz, J. K., and J. R. Baumgardner, 2000: Incremental remapping as a transport/advection algorithm. *J. Comput. Phys.,* **160,** 318–335.

Hack, J. J., J. M. Caron, S. G. Yeager, K. W. Oleson, M. M. Holland, J. E. Truesdale, and P. J. Rasch, 2006: Simulation of the global hydrological cycle in the CCSM community atmosphere model version 3 (CAM3): Mean features. *J. Climate,* **19,** 2199–2221.

Hall, A., 2004: The role of surface albedo feedback in climate. *J. Climate,* **17,** 1550–1568.

Hibler, W. D., III, 1979: A dynamic thermodynamic sea ice model. *J. Phys. Oceanogr.,* **9,** 815–846.

——, 1980: Modeling a variable thickness ice cover. *Mon. Wea. Rev.,* **108,** 1943–1973.

——, 1984: The role of sea ice dynamics in modeling CO_2 increases. *Climate Processes and Climate Sensitivity, Geophys. Monogr.,* Vol. 29, Amer. Geophys. Union, 238–253.

Holland, D. M., L. A. Mysak, D. K. Manak, and J. M. Oberhuber, 1993: Sensitivity study of a dynamic-thermodynamic sea ice model. *J. Geophys. Res.,* **98,** 2561–2586.

Holland, M. M., and J. A. Curry, 1999: The role of physical processes in determining the interdecadal variability of central Arctic sea ice. *J. Climate,* **12,** 3319–3330.

——, J. A. Curry, and J. L. Schramm, 1997: Modeling the thermodynamics of a distribution of sea ice thickness. Part II: Sea ice/ocean interactions. *J. Geophys. Res.,* **102,** 23 093–23 107.

——, C. M. Bitz, and A. J. Weaver, 2001: The influence of sea ice physics on simulations of climate change. *J. Geophys. Res.,* **106,** 19 639–19 655.

Houghton, J. T., Y. Ding, D. J. Griggs, M. Noguer, P. J. van der Linden, X. Dai, K. Maskell, and C. A. Johnson, Eds., 2001: *Climate Change 2001: The Scientific Basis.* Cambridge University Press, 944 pp.

Hunke, E. C., 2001: Viscous-plastic sea ice dynamics with the EVP model: Linearization issues. *J. Comput. Phys.,* **170** (1), 18–38.

——, and J. K. Dukowicz, 1997: An elastic–viscous–plastic model for sea ice dynamics. *J. Phys. Oceanogr.,* **27,** 1849–1867.

——, and ——, 2002: The elastic–viscous–plastic sea ice dynamics model in general orthogonal curvilinear coordinates on a sphere-incorporation of metric terms. *Mon. Wea. Rev.,* **130,** 1848–1865.

Large, W. G., 1998: Modeling and parameterizing the ocean planetary boundary layer. *Ocean Modeling and Parameterization*, E. P. Chassignet and J. Verron, Eds., Kluwer Academic, 81–120.

L'Heveder, B., and M.-N. Houssais, 2001: Investigating the variability of the arctic sea ice thickness in response to a stochastic thermodynamic atmospheric forcing. *Climate Dyn.,* **17,** 107–125.

Lipscomb, W. H., 2001: Remapping the thickness distribution in sea ice models. *J. Geophys. Res.,* **106,** 13 989–14 000.

——, and E. C. Hunke, 2004: Modeling sea ice transport using incremental remapping. *Mon. Wea. Rev.,* **132,** 1341–1354.

Maykut, G. A., 1982: Large-scale heat exchange and ice production in the central Arctic. *J. Geophys. Res.,* **87,** 7971–7984.

——, and N. Untersteiner, 1971: Some results from a time-dependent thermodynamic model of sea ice. *J. Geophys. Res.,* **76,** 1550–1575.

McPhee, M. G., 1992: Turbulent heat flux in the upper ocean under sea ice. *J. Geophys. Res.,* **97,** 5365–5379.

Rayner, N. A., D. E. Parker, E. B. Horton, C. K. Folland, L. V. Alexander, D. P. Rowell, E. C. Kent, and A. Kaplan, 2003: Global analyses of sea surface temperature, sea ice, and night marine air temperature since the late nineteenth century. *J. Geophys. Res.,* **108,** 4407, doi:10.1029/2002JD002670.

Robock, A., 1983: Ice and snow feedbacks and the latitudinal and seasonal distribution of climate sensitivity. *J. Atmos. Sci.,* **40,** 986–997.

Rothrock, D. A., 1975: The energetics of the plastic deformation of pack ice by ridging. *J. Geophys. Res.,* **80,** 4514–4519.

Schramm, J. L., M. M. Holland, and J. A. Curry, 1997: Modeling the thermodynamics of a distribution of sea ice thickness:

Part I. Model description and validation. *J. Geophys. Res.,* **102,** 23 079–23 091.

Steele, M., 1992: Sea ice melting and floe geometry in a simple ice-ocean model. *J. Geophys. Res.,* **97,** 17 729–17 738.

Thompson, D. W., and J. M. Wallace, 2000: Annular modes in extratropical circulation. Part I: Month-to-month variability. *J. Climate,* **13,** 1000–1016.

Thorndike, A. S., D. S. Rothrock, G. A. Maykut, and R. Colony, 1975: Thickness distribution of sea ice. *J. Geophys. Res.,* **80,** 4501–4513.

Timmermann, R., A. Worby, H. Goosse, and T. Fichefet, 2004: Utilizing the ASPeCt sea ice thickness data set to evaluate a global coupled sea ice-ocean model. *J. Geophys. Res.,* **109,** C07017, doi:10.1029/2003JC002242.

Vinje, T., 2001: Fram Strait ice fluxes and atmospheric circulation: 1950–2000. *J. Climate,* **14,** 3508–3517.